Title
INVESTIGATION OF IRON OXIDE REDUCTION BY TEM PART I: HEMATITE REDUCTION

Authors
Rau, M.-F.
Evans, J.W.

Publication Date
1985-07-01

Lawrence Berkeley Laboratory
UNIVERSITY OF CALIFORNIA

Materials & Molecular
Research Division

Submitted to Reactivity of Solids

INVESTIGATION OF IRON OXIDE REDUCTION BY TEM PART I: HEMATITE REDUCTION

M.-F. Rau and J.W. Evans

July 1985

Prepared for the U.S. Department of Energy under Contract DE-AC03-76SF00098

DISCLAIMER

LBL-19960*

Investigation of Iron Oxide Reduction by TEM
Part I: Hematite Reduction

Mann-Fu Rau

and

James W. Evans†

Materials and Molecular Research Division
Lawrence Berkeley Laboratory
and
Department of Materials Science and Mineral Engineering
University of California
Berkeley, CA 94720

†Professor of Metallurgy, to whom correspondence should be addressed.

*Companion paper, LBL-19961, Investigation of Iron Oxide Reduction by TEM. Part II: Magnetite and Wustite Reduction, by M.-F. Rau, D. Rieck, and J.W. Evans.

ABSTRACT

An "environmental cell" located in a high voltage transmission electron microscope has been used to study the reduction of single crystal iron oxides by hydrogen and hydrogen-argon mixtures. The cell enables a direct observation of the solid during reaction, thus permitting the nucleation and growth of solid reaction products to be observed. Part I describes the experimental procedure and results obtained on reducing hematite at temperatures in the range 387 to 610°C with gas pressures up to 40 torr. Reduction with pure hydrogen was considerably faster than when argon was present. Lath magnetite which rapidly transforms to porous magnetite and thence (more slowly) to porous iron, was observed.

INTRODUCTION AND PREVIOUS INVESTIGATIONS

The reduction of iron oxides by hydrogen or carbon monoxide (or their mixtures) is one of the most frequently studied topics in extractive metallurgy. The reader is referred to reviews [1–4] for a detailed account of research carried out on a macroscopic scale, that is on pellets, sinter or lump ore such as are fed to the iron blast furnace or a direct reduction unit. The present investigation is concerned with microstructural aspects of iron oxide reduction, in particular the nucleation, growth and morphology of second solid phases on a scale of micrometers.

Macroscopic studies of iron oxide reduction at temperatures encountered in industrial processes have frequently led to the conclusion that pore diffusion of gases is rate controlling, except for small particles [e.g. 9,10]. The pore diffusion of gases referred to here is the diffusion of gaseous reactants and products through porous reactant or product. The pore structure

(porosity, pore size distribution) is therefore of significance in determining the reaction rate under conditions of pore diffusion or mixed controlled. Turkdogan et al [11] have shown that the structure of the porous iron formed on reduction is very dependent on reduction temperature, being coarser at higher reduction temperature. Koo and Evans [12] showed that the structure of porous iron ores can be markedly altered by holding at temperature prior to reduction. An important microstructural aspect of iron oxide reduction is therefore the development of porosity in solid reaction products.

Edstrom [13] and Edstrom and Bitsianes [14] used optical microscopy to study the relation between microstructure and reduction rate. They observed that the reduction of hematite occurred more rapidly when there was early and extensive formation of pores in the solid reaction products. Brill-Edwards et al [15] studied the reduction of polycrystalline hematite and observed randomly distributed spherical pores for reduction temperatures between 400° and 700°C with elongated pores between 700° and 900°C.

A second microstructural aspect of iron oxide reduction is the nucleation and growth of the solid reaction products. A recent paper on the reduction of wustite is that of El-Rahaiby and Rao [5]. These investigators used polycrystalline specimens of wustite about 50 μm in thickness and carried out hydrogen reduction at 238-417°C. They observed a sigmoidal relationship between extent of reaction and time. That is, on contacting the oxide with the gas there was an initial "incubation" period where little reaction took place, followed by an intermediate period of accelerating reaction rate with a final period of slowing rate. The occurrence of such incubation (or "induction") periods, particularly at lower temperatures, has been noted by

many other investigators for both iron oxide reduction and other gas-solid reactions [12]. A frequent explanation is that the incubation period is due to the nucleation and growth of the second solid phase (iron in the case of wustite reduction). Rao and coworkers [6-8] have recently studied the reduction of magnetite and hematite by similar techniques.

Pluschkell and Yoshikoshi [16] and Rao [17] have used hot stage optical microscopes in investigations of wustite reduction. With these microscopes the nucleation and growth of iron was directly observable under reaction conditions. Bradshaw and Matyas [18] used mercury penetration porosimetry and conventional optical microscopy in a study of the reduction of hematite pellets to magnetite. They suggested that formation of magnetite nuclei could be rate limiting.

St. John and Hayes [19] have used scanning electron microscopy to examine wustite specimens at various stages of reduction by hydrogen or H_2/H_2O mixtures at temperatures from 600 to 1000°C. Faceted pits were observed prior to nucleation of iron when wustite was reduced with 1 atm pure hydrogen at 1000°C. At temperatures below 900°C, pit formation was less pronounced. They noted that pores in the iron product were generally larger as the reducing gas composition approached that of the Fe/FeO equilibrium.

St. John and coworkers [36] have recently reported different results for the reduction of wustite with CO/CO_2 mixtures; the effect of temperature on the product morphology was much less pronounced in this case. However the porosity of the iron formed was dependent on the CO content of the reducing gas. Contrary to the case of hydrogen reduction, these investigators observed

dense iron whiskers on reduction in CO/CO_2 mixtures. They determined that a dense iron layer formed on the surface initially and that, under conditions where porous iron formed, it did so by breakdown of this initial dense layer. St. John et al [37] developed a model for the breakdown of the dense iron layer; the model involved rupturing of the iron layer by gas formed at the iron-oxide interface.

Moukassi et al [20] have shown that the "rate minimum" (a minimum in reaction rate on increasing the reduction temperature), observed in many macroscopic studies of iron oxide reduction, is connected with the evolution of the iron structure towards a dense layer of metal that acts as a barrier to the diffusion of gas.

Some of the investigations cited above have been concerned with the microstructure of iron produced by reduction. In the case of hematite reduction, magnetite is an intermediate reaction product and the microstructure of the magnetite may have a significant effect on the kinetics of the hematite reduction and the subsequent magnetite reduction. Many investigators [15, 21-25] have reported the occurrence of two kinds of magnetite, porous magnetite and dense "lath magnetite", the formation of the latter being favored at high temperatures. Swann and Tighe [23] reported that lath magnetite could act as a nucleus for the growth of porous magnetite but that porous magnetie could also be formed without prior formation of lath magnetite.

The electron microscope provides a convenient means for study of microstructural aspects of gas-solid reactions and has been used in several of

the investigations referred to above. With the exception of the work of Swann and collaborators [23, 24], all such investigations have made "ex-situ" examinations of the solid specimens. In this method specimens are exposed to the reactive gas at temperature and then withdrawn from that environment to be placed in the electron microscope. The method has the disadvantage that structural changes, or even reaction, can ocur as the specimen is cooled and transferred to the microscope. Even if the rapid quenching procedure, described by Hayes and coworkers [19], is used there exists the possibility that the microstructure seen in the microscope differs from that under reaction conditions. Furthermore, although a specimen can usually be returned to the reaction apparatus, enabling the microstructure of the specimen to be examined at various stages in the reaction, it is frequently difficult to relocate the same region of the specimen because of obliteration of recognizable features of the specimen as reaction proceeds. A technique for overcoming this difficulty in ex-situ studies has been described by Little et al [26].

The alternative to ex-situ studies is the use of an "environmental cell" within the electron microscope. Studies with such a device (described more fully below) are "in-situ" investigations or are frequently referred to by the acronym CAEM (controlled atmosphere electron microscopy). The technique has been employed to study reactions in scanning electron microscopes [e.g. 27, 28] but of interest in the present investigation is its use in transmission electron microscopy. In-situ studies of gas-solid reactions have included investigations of carbon gasification [29-31], chemical vapor deposition reactions [32], oxidation of gallium arsenide [33] and the thermal decomposition of ammonium salts [34]. Swann and coworkers [23, 24] have made

considerable use of the in-situ technique in their study of the reduction of hematite to magnetite in H_2-He and CO-CO_2 mixtures. The present investigation has used the technique to study other iron oxide reduction reactions. Part I of this two part paper describes the experimental technique and results on the reduction of hematite. Part II presents results on the reduction of magnetite and of wustite.

EXPERIMENTAL APPARATUS AND PROCEDURE

Most of the microscopy of this investigation was carried out on the Hitachi HU-650 transmission electron microscope at Lawrence Berkeley Lab. Occasional use was made of the Kratos EM-1500 electron microscope at the same location. Both microscopes have environmental cells (Gatan Co.) with hot stages and a single tilt axis. Figure 1 is a schematic diagram illustrating the principles of the environmental cell. The electron microscope can only form an image of the specimen if little absorption or scattering of electrons occurs as the electrons pass through the column of the instrument. The normal electron microscope is therefore unsuitable for observing the interaction of a gas with a solid since the gas would absorb and scatter the electrons. The environmental cell permits such an observation by limiting the path length of the electron beam through the gas to a few millimeters. This is sufficiently short that image quality is only slightly impaired although quality deteriorates as the gas pressure is raised or the electron capture cross section of the gas molecule increases. The environmental cell has four apertures (of 100 μm nominal diameter), two located above the specimen and two below. The apertures are sufficiently small that little leakage of gas occurs through the apertures closest to the specimen and most of this leaked gas is diverted to auxiliary vacuum pumps connected to the space between inner and

outer apertures. Leakage of gas through the outer apertures and into the microscope column is then small and can be accommodated by the main column pumps.

The heating element in the environmental cell was a 0.003 inch platinum wire wound into a coil of 45 turns and surrounded by a ceramic cement (Aremco 503) as an insulator (see Figure 2). This coil was located on the outside of the body of the furnace which was made of Inconel. The specimen was supported on a standard 3mm diameter nickel grid which was pressed against the furnace body by a retaining screw. The furnace temperature was measured by a Pt/Pt-13% Rh thermocouple attached to the outside of the furnace (but beneath the ceramic insulation). The heater was driven by a power supply (Gatan Co.) capable of regulated current. Calibration curves of furnace temperature versus current were determined in the various gas environments used in this investigation. The accuracy of the heater and thermocouple was tested using two TEM samples made of 6% Cu-94% Al. The TEM specimens were heated until the θ phase precipitates disappeared. The θ precipitates disappeared in one specimen at 552°C; in the other specimen the θ precipitates disappeared at 560°C. Aluminum alloys with 6% Cu are single phase at temperatures above 548°C. From the above tests it is seen that temperatures within approxiately 10°C of the measured temperature can be achieved [38].

Figure 3 is a schematic diagram of the gas supply system used in this investigation. Gas from a cylinder flowed via a regulator, flowmeter (Hastings NALL-500) and valves to the environmental cell. Pressure was measured at a point just before the gas entered the cell using a SPEEDVAC pressure gauge (Edwards High Vacuum Type C.G.3).

Wustite single crystals used in this investigation were obtained from Purdue University and were prepared by skull melting [35]. Magnetite single crystal slab was prepared by Argonne National Lab. Hematite single crystal was available at Lawrence Berkeley Lab but of unknown source. The hematite sample was subjected to spectrographic analysis and showed a few impurities at the level of a few tens of parts per million. Gases used in the investigation were obtained from Lawrence Berkeley Lab. A mass spectrometer was used to check the impurity levels of some gas cylinders; only trace amounts of impurities were found.

Specimens of all three oxides were prepared in the same way. Discs approximately 1 mm thick were cut using a diamond saw and mounted on one inch diameter quartz discs. The iron oxides were then ground (#600 silicon carbide paper) and polished (6 μm followed by 1 μm diamond paste). The discs were then turned over and ground and polished on the reverse to a thickness of approximately 50 μm. The iron oxide discs were then cut into pieces between 1 and 2 mm on edge and each mounted on 3 mm grids using a ceramic adhesive (Aremco 503). Finally the specimens were thinned in an ion mill until a hole appeared. In the case of wustite, which is thermodynamically unstable below 570^{o}C, a cold stage was used during the iron thinning.

After loading a specimen into the environmental cell and pumping down the microscope, photomicrographs of the initial specimen were taken. Thereafter the flow of gas from the gas supply was commenced and time allowed for purging of gas lines and the establishment of stable pressures (approximately ten minutes). The heater current was then switched on and set to the required

value; the reaction temperature was achieved typically in less than ten seconds. Photomicrographs were taken as the reaction proceeded. Reaction was halted (by turning off the power) after only partial reaction because of the danger of porous reaction products falling apart. Some specimens were examined subsequent to reduction; such ex-situ examinations permitted a more complete structural analysis than was possible in-situ.

RESULTS AND DISCUSSION

Swann and coworkers [23,24] have studied the reduction of hematite but their published results are confined to the reduction to magnetite. The present investigation is concerned with this reduction and the subsequent reduction to iron.

Reduction with pure hydrogen

Figure 4 shows the appearance of an edge of the sample before and after exposure to 2 torr of pure hydrogen at 387°C for 220 seconds. Little or no reaction was observed in the first 150 seconds and thereafter reaction was observed to proceed rapidly. This is consistent with results from macroscopic studies of hematite reduction where an incubation period is reported [22]. The dark lines paralleling the edge of the specimen in the upper figure are thickness contours arising from the tapering of the specimen towards its edge. They are an interference effect and have no physical significance. The small dark grains in this micrograph were identified from the electron diffraction pattern as magnetite that may have been formed during ion thinning. This amount of magnetite is small and, as will be seen below, is unlikely to have affected the reaction.

Figure 5a is the electron diffraction pattern for the central region of Figure 4 after 220 seconds exposure to hydrogen. The "spotty" ring pattern corresponds to polycrystalline magnetite. Figure 5b is the diffraction pattern for a region to the right of Figure 4 and reveals the presence of polycrystalline iron. This region of the edge of the specimen was the point at which reaction was seen to start and sweep across the surface of the specimen.

Figure 6 is an area adjacent to and to the right of the region depicted in Figure 4. Note that this sequence of micrographs was taken at lower magnification than those of Figure 4; time in seconds is indicated. The bright areas appearing in the sample are pores and the development of an individual pore, indicated by the arrow, is clearly seen.

An (ex-situ) overview of a whole reaction zone after 880 seconds is presented as Figure 7; this is a region not previously struck by the electron beam. The dark band is lath magnetite separating the inner porous mass of magnetite and iron from unreacted single crystal hematite. The minute black grains on the hematite are those initially present that were mentioned above; they have not become sites for reaction. Figure 7 creates an impression of "topochemical" reaction such as is frequently observed in macroscale studies of gas-solid reactions. It should be noted however that, because the specimen is a thin foil, reaction is starting at an edge rather than on the surface, and subsequently propagating through the body of the sample.

Figure 8 shows the diffraction patterns from various regions of Figure 7. The diffraction patterns were taken with a 500 nm aperture centered about the points indicated by the lines. Region (a) is identified as iron, while the

other three regions have the diffraction pattern corresponding to magnetite. A schematic diagram of a cross section of the foil appears as Figure 9. Region I is predominantly porous iron; in region II porous magnetite is the predominant phase and the shrinkage resulting from the lower volume of magnetite (compared to hematite on a per mole of iron basis) results in this region having high porosity. Region III has lower apparent porosity due to residual hematite. It is conjectured that the lack of porosity of the lath magnetite may be a consequence of this phase existing as thin sheets that can accommodate the volume change by transverse shrinkage.

In their ex-situ studies of hematite reduction, Swann and Tighe noted that porous magnetite is the product of hematite reduction at temperatures below 650°C and that lath magnetite results from reduction above 850°C. Baguley et al [25] noted that lath magnetite was observed in the initial stages of reduction at 400°C and that the lath magnetite acted as nucleation sites for subsequent growth of the porous magnetite. Figure 10 shows a specimen reduced under the same conditions as that of Figure 4 for 220 seconds. In this instance no lath magnetite can be seen.

The reaction fronts were seen to slow down as they moved into thicker regions of the sample. The width of the layer of lath magnetite stayed constant at approximately 1 μm. This suggests that lath magnetite is a short lived intermediate in the reduction and that the formation of lath magnetite from hematite and its transformation to porous magnetite are not rate controlling; the slow reduction of porous magnetite to iron is indicated by the large amount of porous magnetite observable in micrographs such as Figure 8. This confirms the results of Rao and Moinpour [22] who studied reduction

of hematite with pure hydrogen in the temperature range 245-482°C and noted that the rate controlling step appears to be the conversion of magnetite to iron.

There is a possibility of the reduction reactions being affected by the presence of the electron beam, perhaps as a consequence of heating of the specimen by the beam or because of radiation damage. Initiation of reaction always occurred in a region of the hematite struck by the beam although it also occurred in other regions. Advancement of the reaction fronts appeared to proceed more rapidly in the regions illuminated by the beam but the morphology of the reaction products was not significantly affected. None of the samples examined showed evidence of wustite formation during reduction which is consistent with the thermodynamic instability of this oxide below 570°C.

At the temperatures employed in this investigation little change occurs in the structure of the porous iron product. Figure 11 shows a region that is predominantly iron 3 minutes (a) and 14 minutes (b) after the original hematite was contacted with 2 torr hydrogen at 417°C. Note that the morphology changes little in the 11 minute interval except near the point X where some enlargement of pores and reaction of residual magnetite is discernible.

Reduction with a hydrogen/argon gas mixture

Using 10% H_2/90% Ar as reducing gas, preliminary experiments were carried out using temperatures and pressures in the ranges employed with pure

hydrogen. Reaction was too slow and subsequent experiments were carried out at 40 torr total pressure and higher temperatures. Even then, hematite reduction was much slower than observed using pure hydrogen.

Figure 12 is a stereo pair showing the appearance of the edge region of a specimen exposed to this gas mixture at 610°C for 480 seconds. Reaction was observed to occur across the whole surface, rather than starting at an edge and sweeping across the surface. Examination of Figure 12 with a stereo viewer reveals that there are no pores present.

Figure 13 shows bright (a) and dark (b) field images of magnetite produced by 10 minute exposure at these conditions. Diffraction patterns (c) and (d) were taken from the center and tip of the region shown in Figure 13a. The diffraction patterns reveal that neither iron nor wustite are present in the specimen although some samples reduced at this temperature showed inconclusive evidence of wustite.

Three possible explanations can be advanced for the slower reaction observed in the presence of argon:

(a) mass transfer limitations with argon present

(b) blockage of reaction sites by adsorbed argon

(c) a lower sample temperature in the presence of argon.

Estimation of a mass transfer coefficient is precluded by the complicated geometry of the cell and the microscopic nature of the sample. However, the diffusion coefficient for H_2-H_2O at 2 torr total pressure, 387°C is estimated to be 1277 cm^2/s from the Fuller et al correlation [39] while that for H_2-Ar

at 40 torr, 610°C is 100 cm^2/s. The mass transfer coefficient would be enhanced by the higher flow rate through the environmental cell in the presence of argon (higher total pressure and therefore higher leakage through the cell apertures) and potential mass transfer rates would be further enhanced by the higher concentration driving force. It therefore seems possible that the slower rate can be ascribed to the presence of argon in the gas phase. Explanation (b) also appears unlikely since neither chemical nor physical adsorption of argon is expected under these experimental conditions. Finally explanation (c) is made unlikely by the fact that the heat required to bring the flowing gas from room to reaction temperature is less than 2 percent of the heat generated electrically in the environmental cell for the case of argon present.

CONCLUSIONS

In situ studies of hematite reduction have been carried out using hydrogen and using a hydrogen/argon mixture. Reduction by hydrogen was faster and started from nucleation sites on the edge of the sample. Four clearly distinguishable zones were revealed; unreacted single crystal hematite which usually forms lath magnetite under the conditions of the study, the lath magnetite which rapidly transforms to porous magnetite, porous magnetite and porous iron. The rate controlling step appears to be the reduction of magnetite to iron. Reduction with the hydrogen/argon mixture proceeded much more slowly and across the whole surface, producing granular magnetite.

ACKNOWLEDGMENT

This work was supported by the Director, Office of Energy Research, Office of Basic Energy Sciences, Materials Sciences Division of the U.S. Department of Energy under Contract Number DE-AC03-76SF00098.

REFERENCES

1. L. von Bogdandy and H. J. Engell: The Reduction of Iron Ores, Springer-Verlag, Berlin (1971).
2. J. W. Evans and C. H. Koo: In Rate Processes of Extractive Metallurgy, H. Y. Sohn and M. E. Wadsworth (Eds.), Plenum Press, New York (1979), p.286.
3. J. Szekely, J. W. Evans and H. Y. Sohn: Gas-Solid Reactions, Academic Press, New York (1976), p.338.
4. E. T. Turkdogan and J. V. Vinters: Metall. Trans. 2(1971), p.3175.
5. S. K. El-Rahaiby and Y. K. Rao: Metall. Trans. 10B(1979), p.257.
6. Y. K. Rao and M. Moinpour: Metall. Trans. 14B(1983), p.711.
7. M. M. Al-Kahtany and Y. K. Rao: Ironmaking and Steelmaking 7(1980), p.49.
8. S. K. El-Rahaiby and Y. K. Rao: Trans. ISIJ 20(1980), p.287.
9. E. T. Turkdogan and J. V. Vinters: Metall. Trans. 3(1972), p.1561.
10. J. W. Evans and K. Haase: High Temp. Sci. 8(1976), p.167.
11. E. T. Turkdogan, R. G. Olesson and J. V. Vinters: Metall. Trans. 2(1971), p.3189.
12. C. H. Koo and J. W. Evans: Trans. ISIJ,
13. J. O. Edstrom: J. Iron & Steel Inst. 175(1953), p.289.
14. J. O. Edstrom and G. Bitsianes: AIME Trans. 203(1955), p.760.
15. H. Brill-Edwards, B. L. Daniell and R. L. Samuel: J. Iron & Steel Inst. 203(1965), p.361.
16. W. Pluschkell and H. Yoshikoshi: Arch. Eisenhuttenw. 41(1970), p.715.
17. Y. K. Rao: Metall. Trans. 10B(1979), p.243.
18. A. V. Bradshaw and A. G. Matyas: Metall. Trans. 7B(1976), p.81.
19. D. H. St. John and P. C. Hayes: Metall. Trans. 13B(1982), p.117.

20. M. Moukassi, P. Steinmetz, B. Dupre and C. Gleitzer: Metall. Trans. 14B(1983), p.125.

21. P. C. Hayes and P. Grieveson: Metall. Trans. 12B(1981), p.579.

22. A. Unal and A. V. Bradshaw: Metall. Trans. 14B(1981), p.743.

23. P. R. Swann and N. J. Tighe: Metall. Trans. 8B(1977), p.479.

24. J. R. Porter and P. R. Swann: Ironmaking & Steelmaking 5(1977), p.300.

25. P. Baguley, D. H. St. John and P. C. Hayes: Metall. Trans. 14B(1983), p.513.

26. J. A. Little, M. I. Perez and J. W. Evans: Lawrence Berkeley Lab Report no. LBL-11473 (1980).

27. U. Finnstrom: Scand. J. Metall. 5(1976), p.134.

28. R. A. Rapp: Metall. Trans. 15A(1984), p.765.

29. R. T. K. Baker and P. S. Harris: J. Phys. E. 5(1972), p.793.

30. D. J. Coates, J. W. Evans, A. L. Cabrera, G. A. Somorjai and H. Heineman, J. Catalysis 80(1983), p.215.

31. D. J. Coates, J. W. Evans and H. Heinemann, J. Appl. Catalysis 7(1983), p.233.

32. T. Gabor and J. M. Blocher: J. Vac. Sci. Technol. 6(1969), p.815.

33. M. E. Hall: In-Situ Study of GaAs Oxidation, M.S. Thesis, LBL-18902, Lawrence Berkeley Laboratory, U.C. Berkeley (1985).

34. H. Hashimoto, S. Urai, H. Yotsumoto and J. Sawamori: In Proc. 7th Int. Congr. Electron Microscopy, Grenoble, 2(1970), p.399.

35. H. R. Harrison, R. Aragon and C. J. Sandberg: Mat. Res. Bull. 15(1980), p.571.

36. D. H. St. John, S. P. Mathew and P. C. Hayes: Metall. Trans. 15B(1984), p.709.

37. Ibid, p.701.

38. Bulletin of Alloy Phase Diagrams, Vol. 1, No. 1, p. 29.

39. E. N. Fuller, P. D. Schettler and J. C. Giddings: Indust. and Eng. Chem. 58(1966), p. 19.

FIGURE CAPTIONS

Fig. 1 Schematic diagram of 'environmental cell'. Note that the electron beam passes through four 100 m apertures.

Fig. 2 Schematic diagram of specimen hot stage.

Fig. 3 Schematic diagram of the experimental set-up. The flow meter was disconnected when the flowrate-pressure calibration was accomplished.

Fig. 4 Electron micrographs of hematite specimen before (a) and after (b) reducing in 2 torr pure hydrogen at 387°C for 3 min and 40 sec. The product phases include porous iron (right), polycrystalline magnetite (center) and pores (left).

Fig. 5 Typical electron diffraction pattern for (a) the center part of the region in Figure 4 showing that only polycrystalline magnetite exists, and (b) to the right of the region revealing that porous iron coexists with polycrystalline magnetite.

Fig. 6 Sequence electron micrographs revealing the development of pores during hematite reduction by 2 torr pure hydrogen at 387°C. The numbers inserted are the reduction time in seconds.

Fig. 7 Typical configuration of reaction zones after hematite reduction using pure hydrogen. The specimen was reduced by 2 torr H_2 at 387°C for 14 min and 40 sec.

Fig. 8 Selected area diffraction patterns from different reaction zones. Corresponding structures are porous iron (a), polycrystalline magnetite (b) and (c), and lath magnetite (d). The hematite specimen was reduced by 2 torr pure H_2 at 387°C for 14 min and 40 sec.

Fig. 9 Schematic diagram of the cross-section of the specimen illustrating five different zones corresponding to Figure 8.

Fig. 10 Morphology of a partially reduced hematite specimen obtained under the

same reducing conditions as Figure 4(b). Lath magnetite was not found in this case.

Fig. 11 Electron micrographs of porous iron obtained by reducing hematite with 2 torr pure hydrogen at 417°C for 3 min (a) and 14 min (b). Note that a large portion of the morphology is unchanged except the area near the marker 'X' where the retraction of the residual magnetite and the enlargement of pore size can be seen.

Fig. 12 Stereo pair of electron micrographs revealing the crystalline morphology of hematite after 8 min reduction under 40 torr of 10% H_2/ 90% Ar mixture at 610°C. Note that no pores were developed.

Fig. 13 Bright (a) and dark (b) field images of magnetite product after 10 min reduction time under the same conditions as above. Diffraction patterns (c) and (d), corresponding to [122] and [111] zone axes of magnetite single crystal patterns, were taken from the center and the tip of (a), respectively.

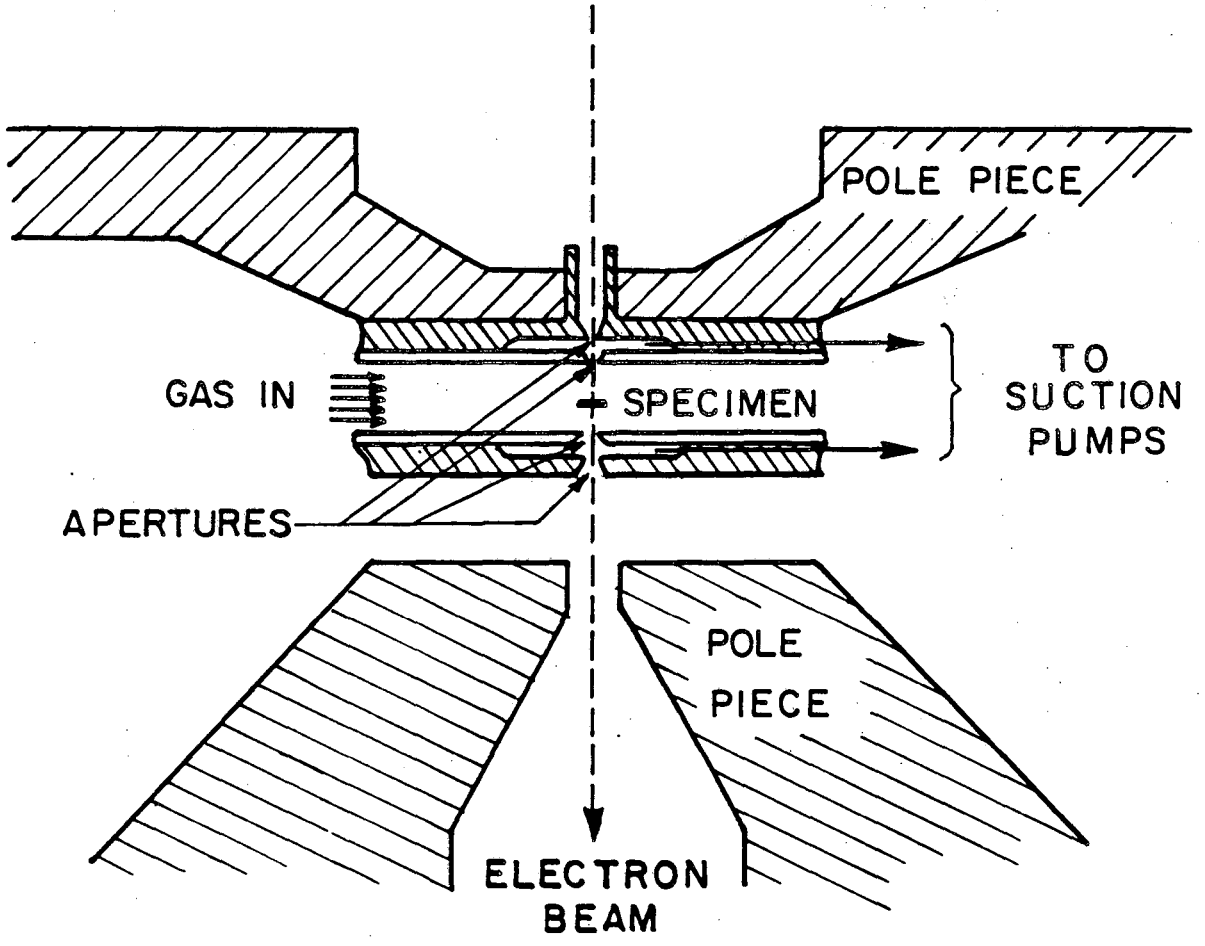
POLE PIECE
GAS IN
SPECIMEN
TO
SUCTION
PUMPS
APERTURES
POLE
PIECE
ELECTRON
BEAM
XBL 791-5538

Figure 1.

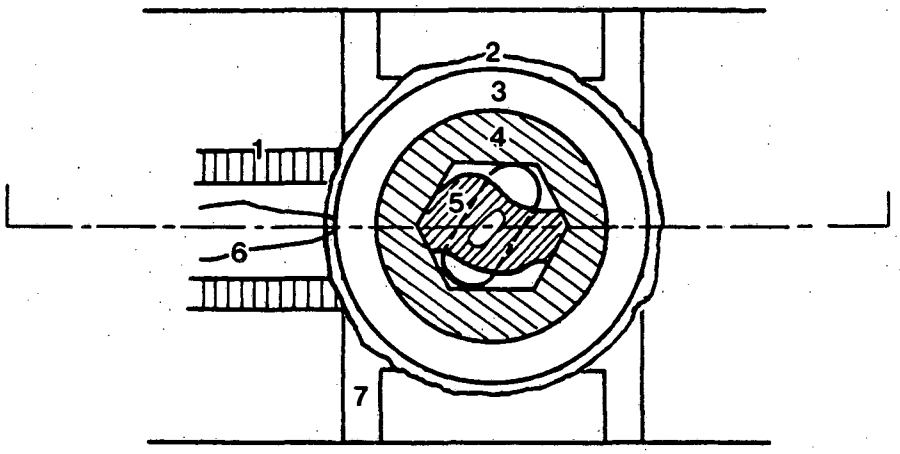

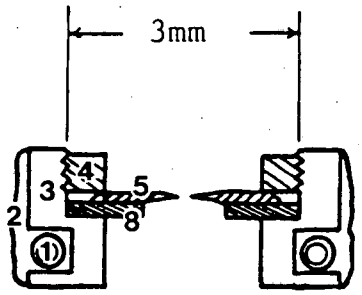

1. heating wire
2. insulating ceramic
3. furnace
4. screw
5. specimen
6. thermocouple
7. support
8. nickel grid

XBL 8412-5452

Figure 2.

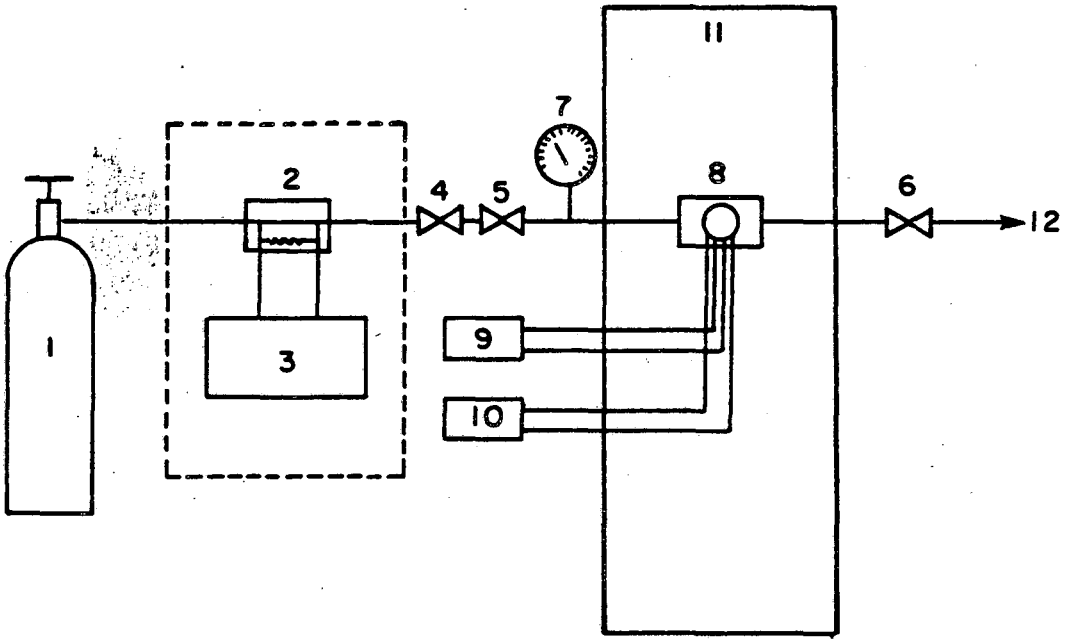

1. gas mixture
2. transducer
3. digital flowmeter
4. gate valve
5. needle valve
6. gate valve
7. pressure gauge
8. E-cell
9. thermocouple
10. power supply
11. HVEM
12. to mechanical pump

XBL 8412-5450

Figure 3.

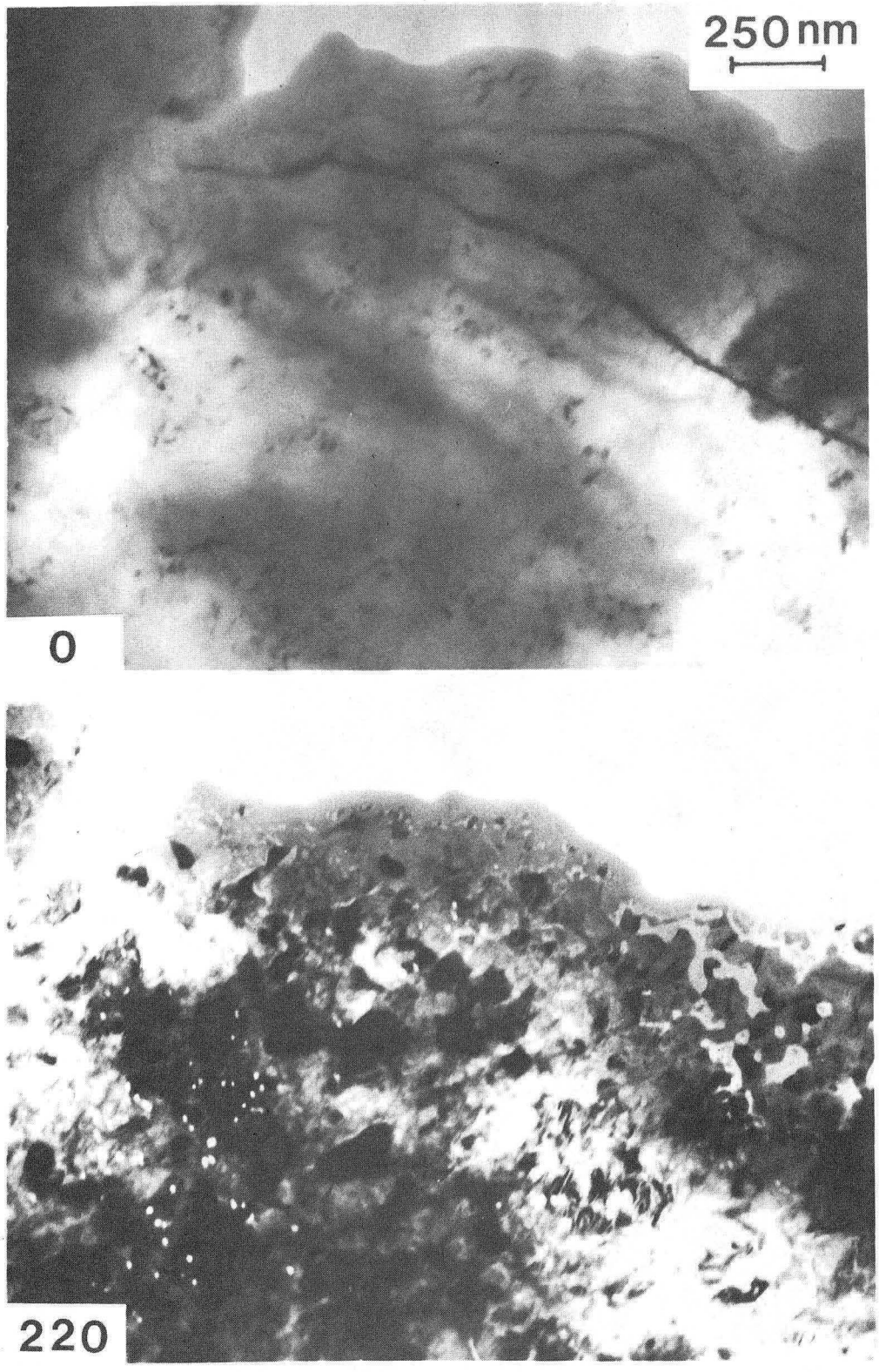

Figure 4.

XBB 840-9182

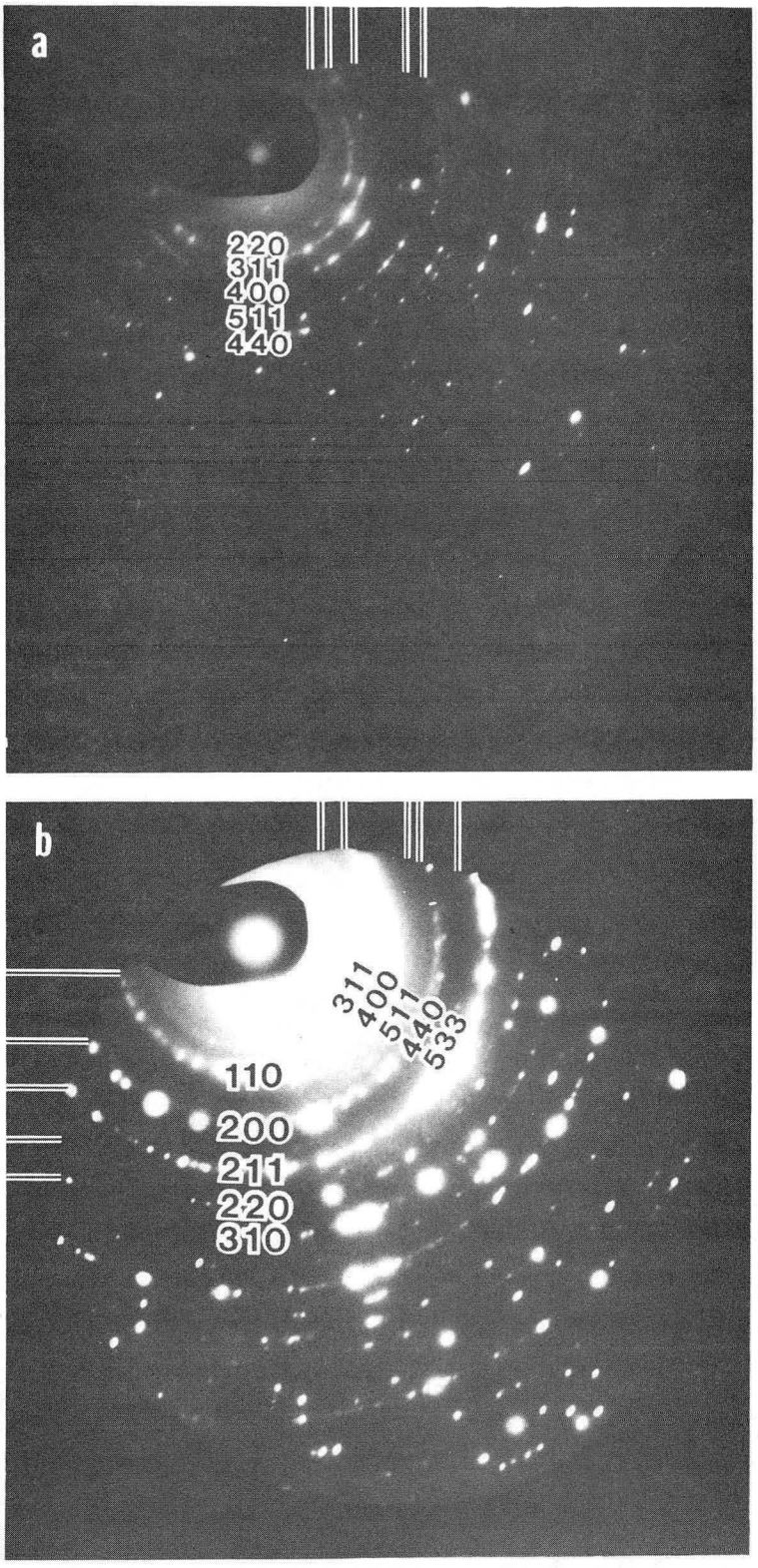

Figure 5.

XBB 840-9598

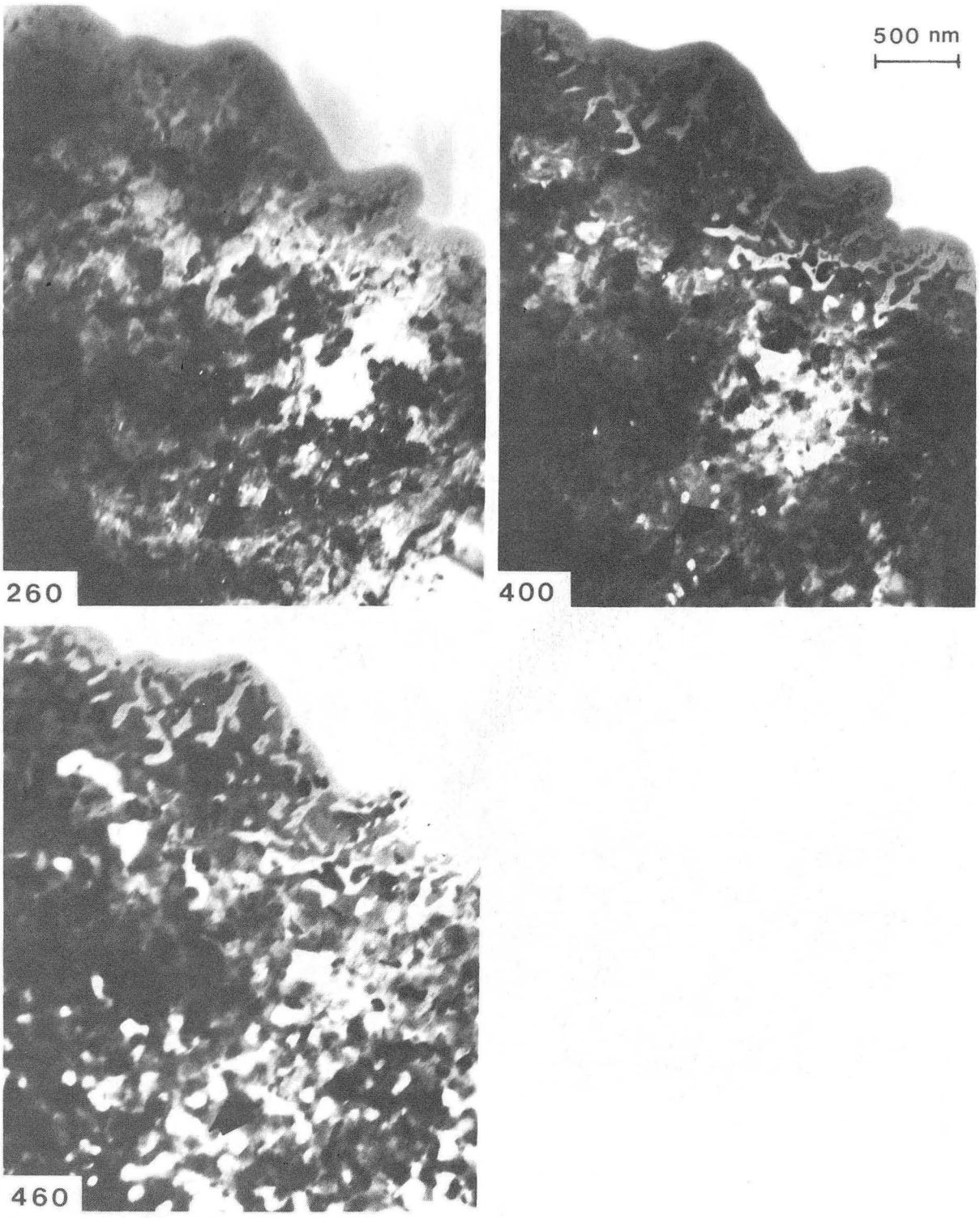

Figure 6.

XBB 840-9599

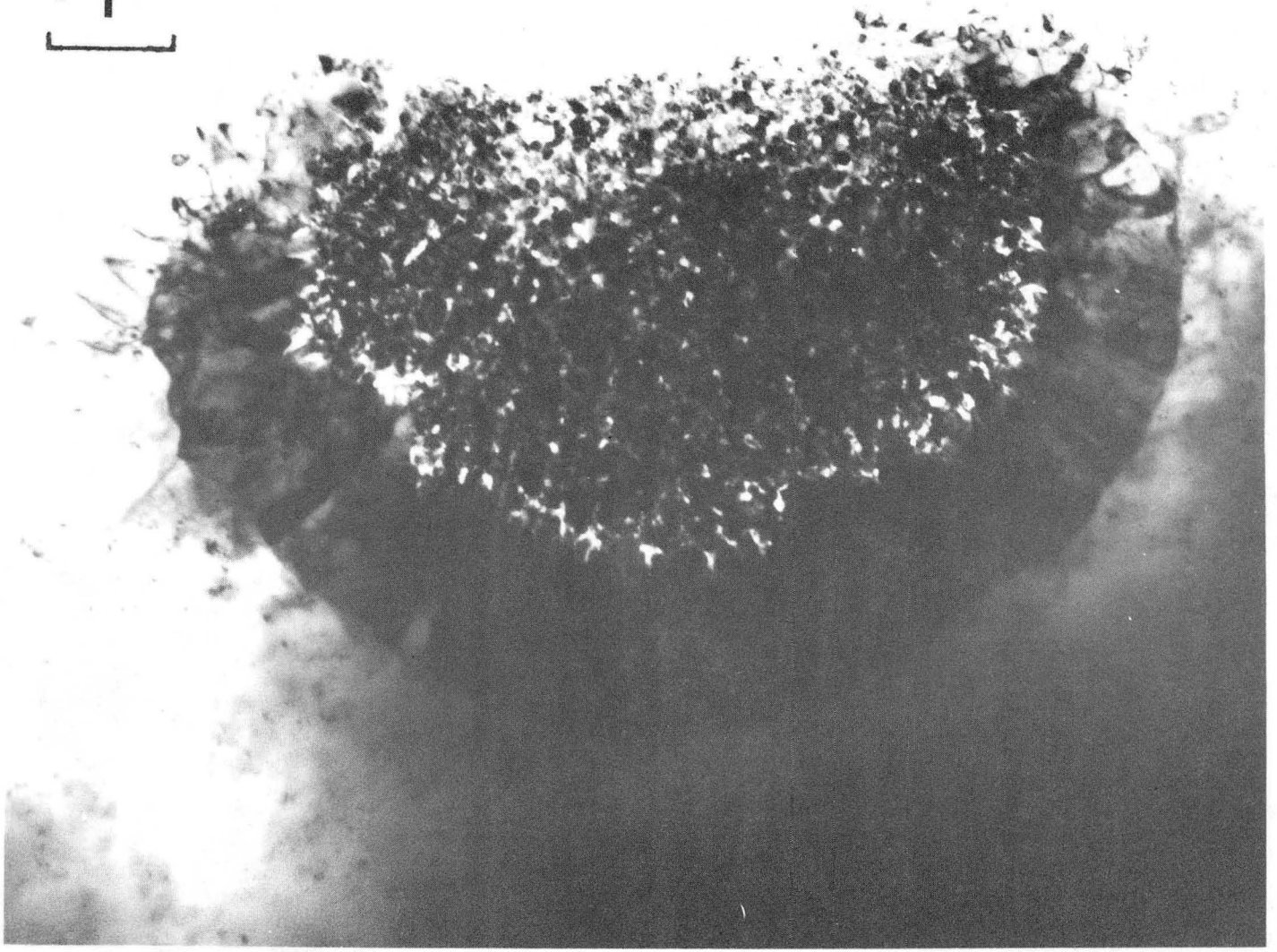

Figure 7.
XBB 840-9600

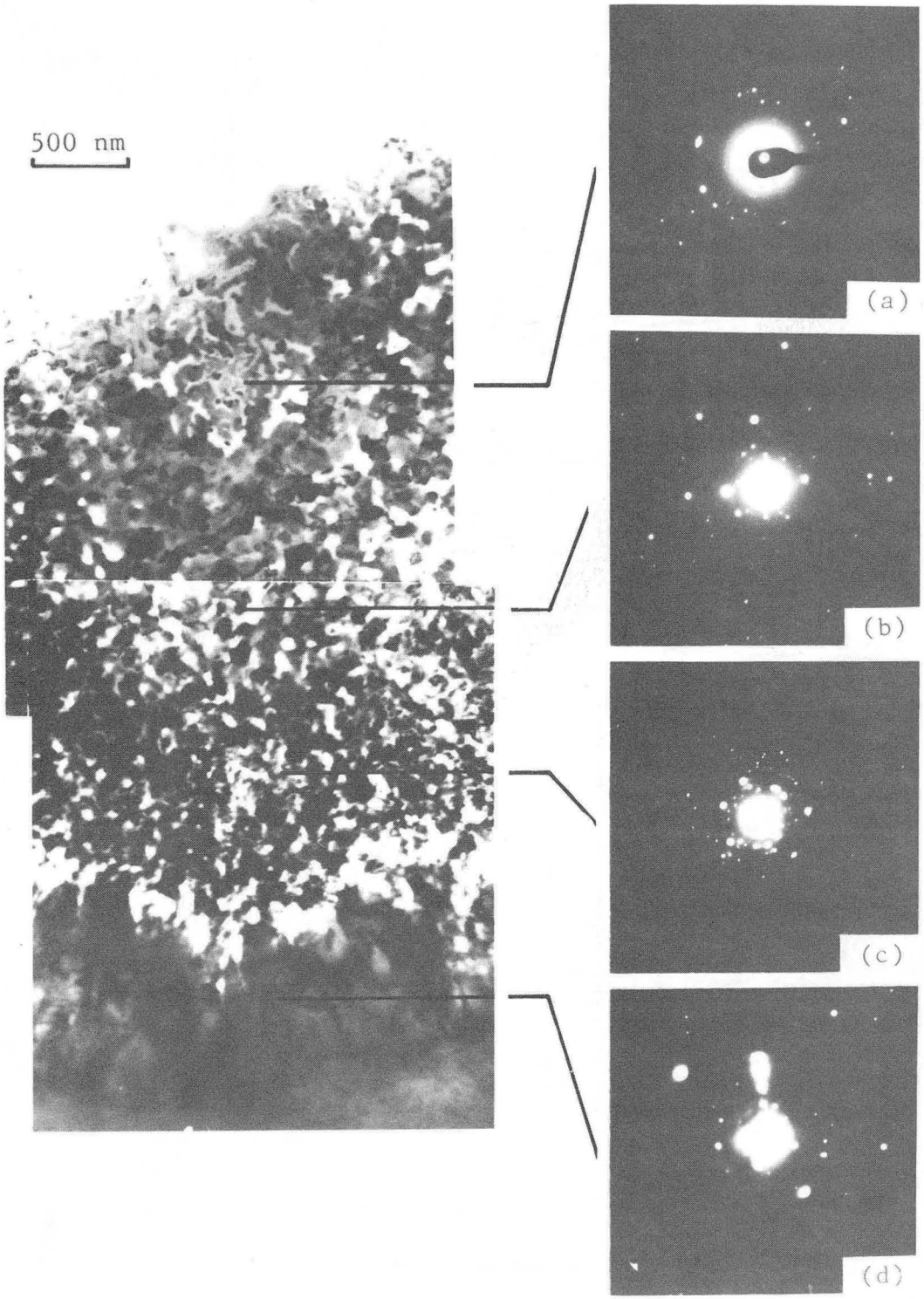

Figure 8.

XBB 840-9585

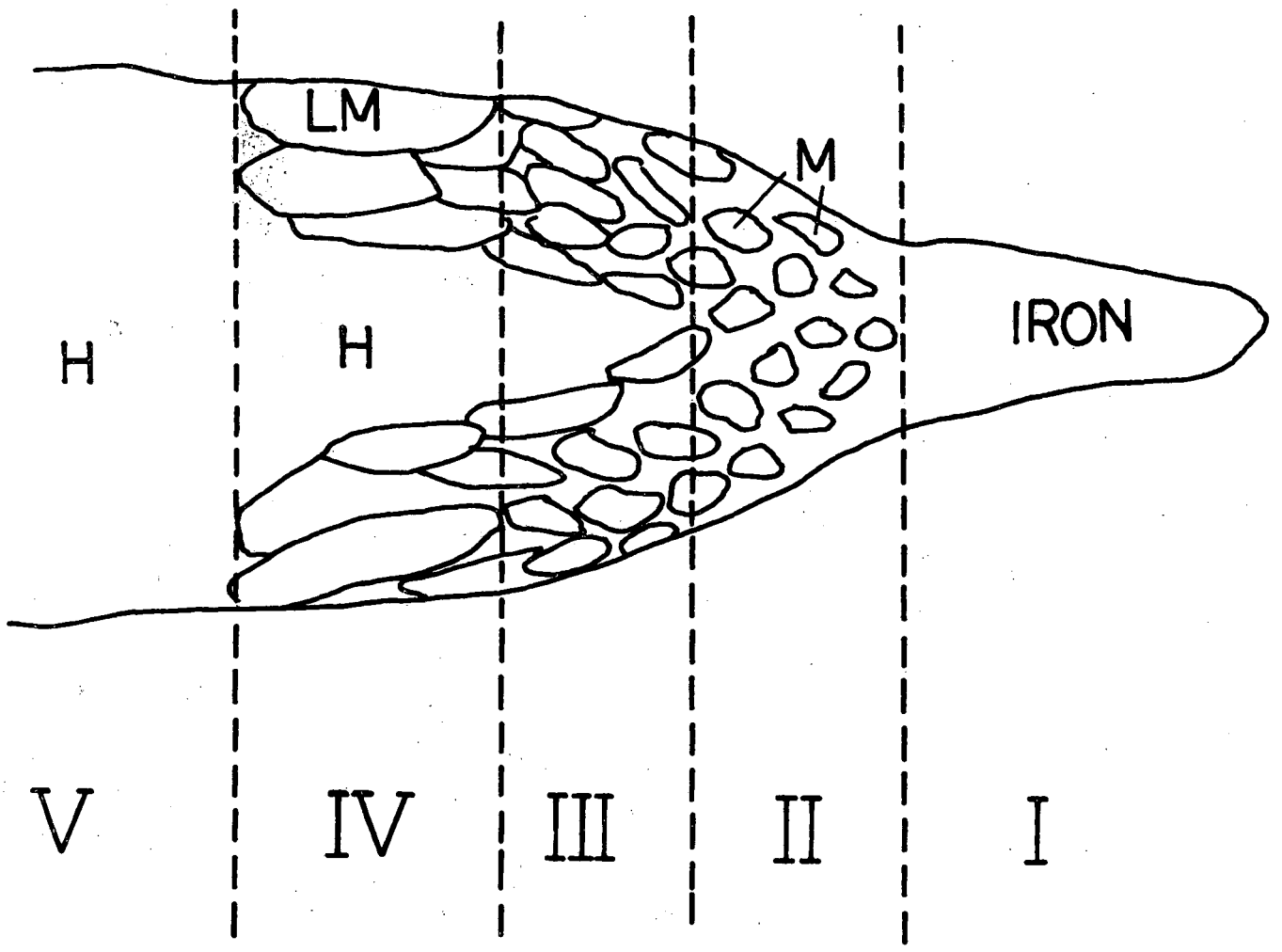

XBL 8412-5449

Figure 9.

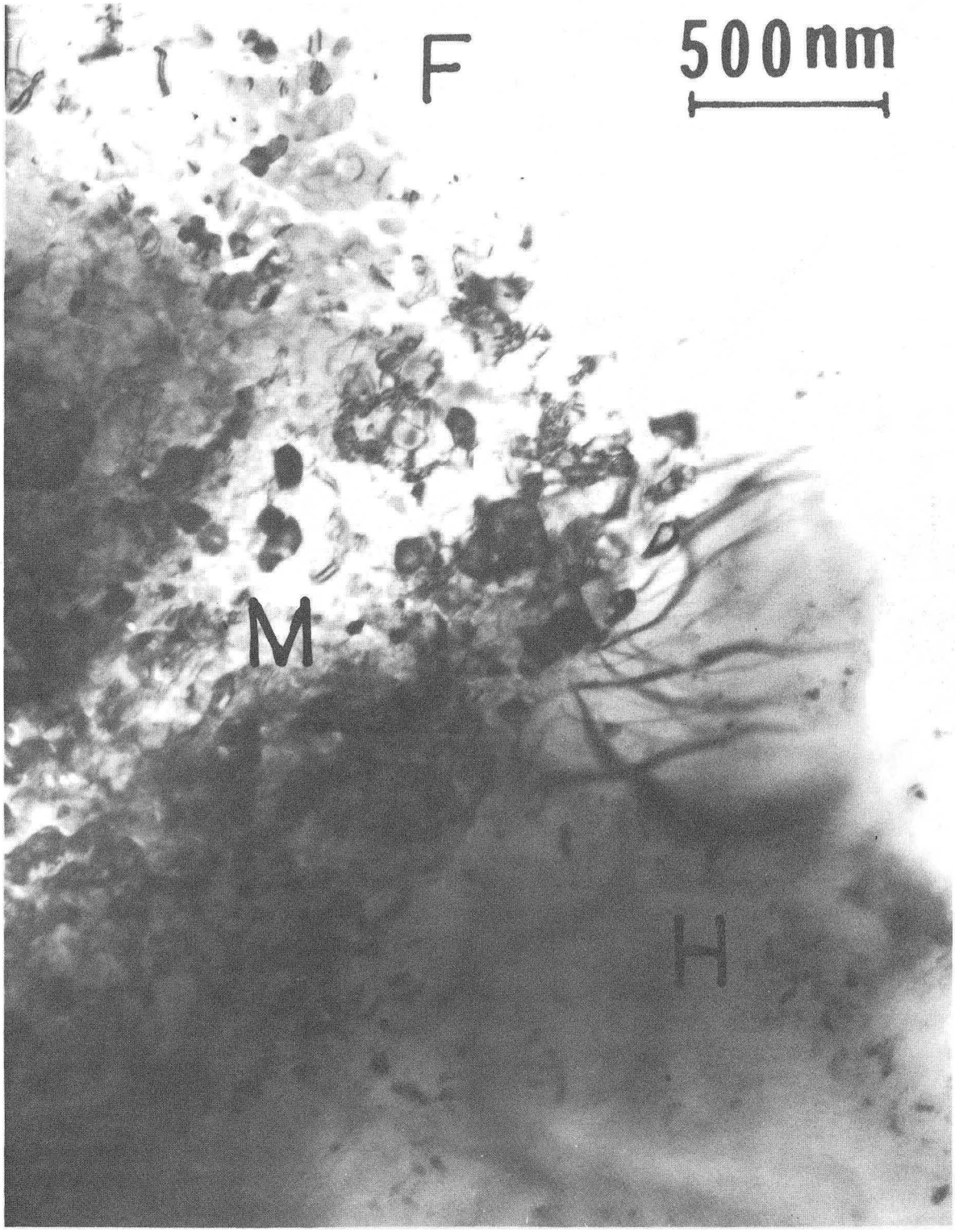

Figure 10.
XBB 840-9583

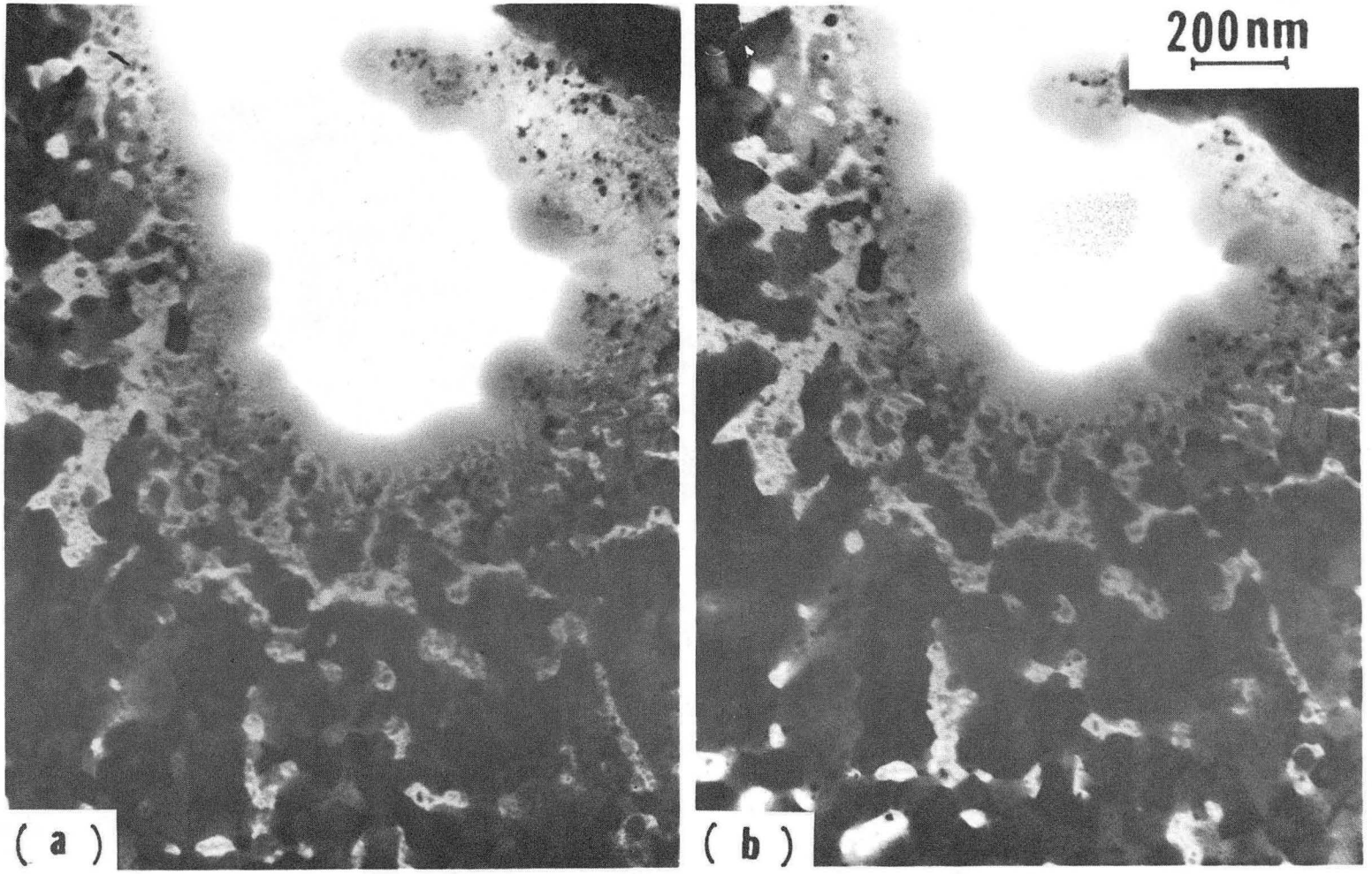

Figure 11.

XBB 840-9596

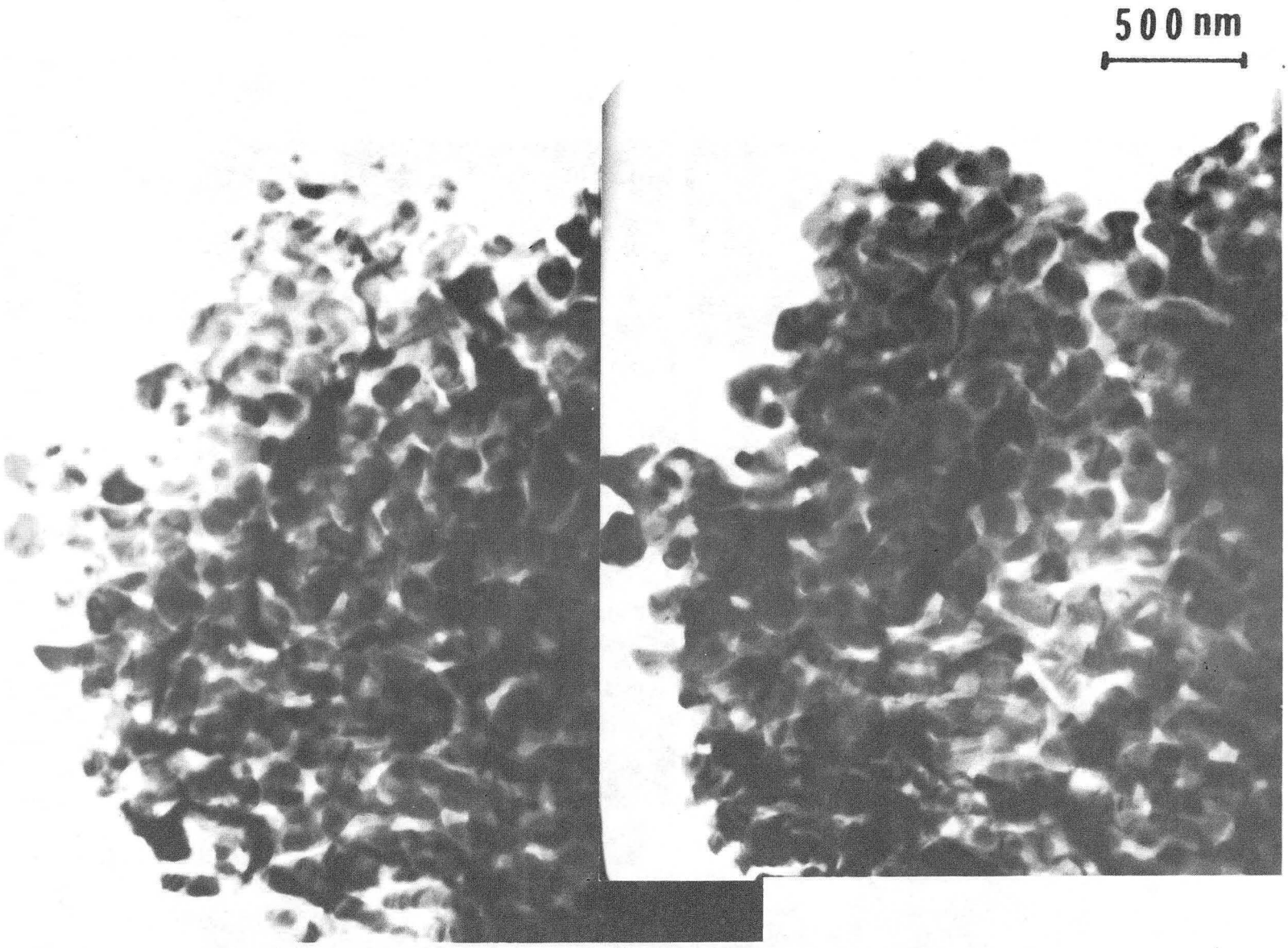

Figure 12.

XBB 840-9587

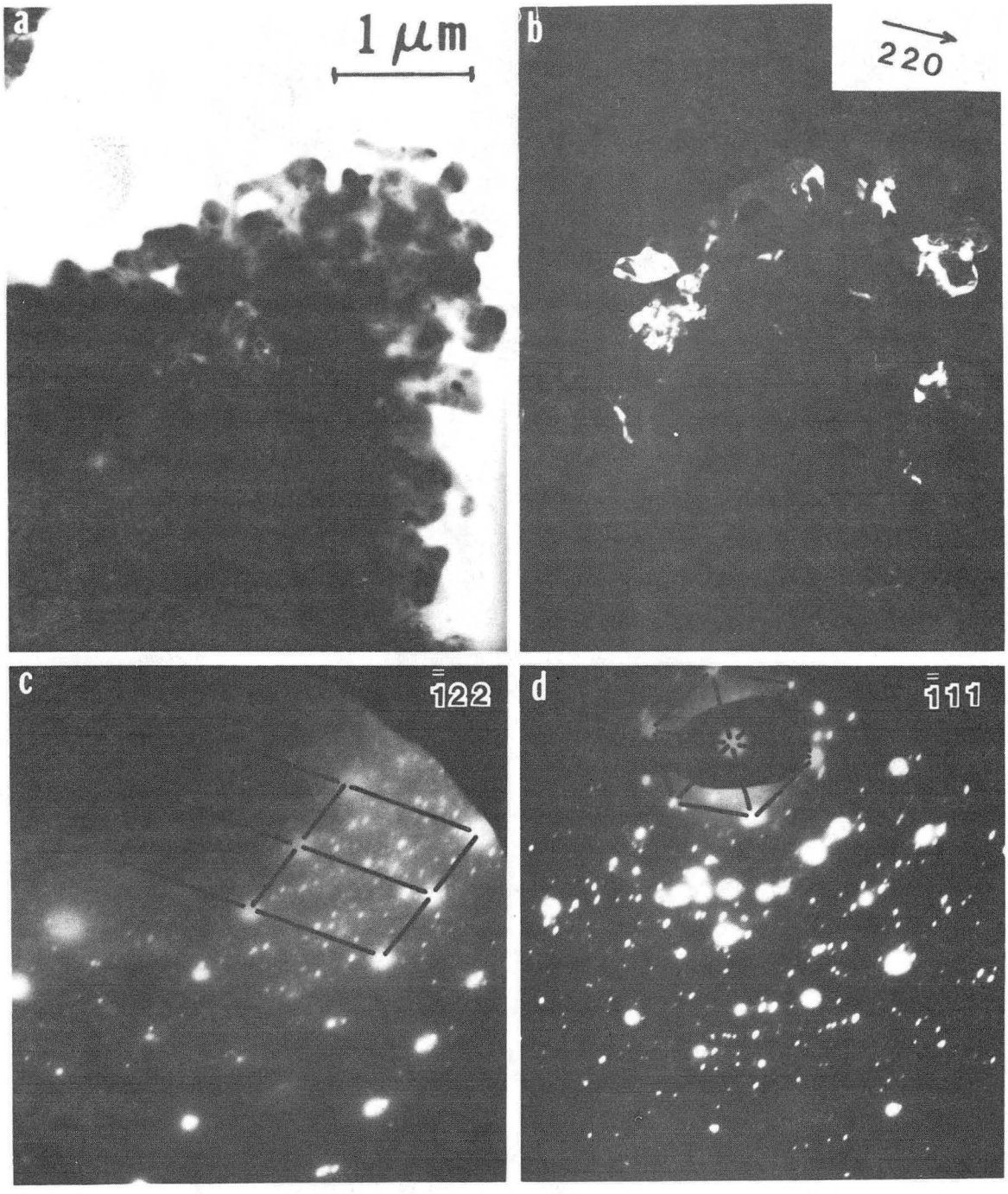

Figure 13.

XBB 840-9624

LAWRENCE BERKELEY LABORATORY
TECHNICAL INFORMATION DEPARTMENT
UNIVERSITY OF CALIFORNIA
BERKELEY, CALIFORNIA 94720